

Recent irreversible retreat phase of Pine Island Glacier

Reed, Brad; Green, Mattias; Jenkins, Adrian; Gudmundsson, Hilmar

Nature Climate Change

DOI:
[10.1038/s41558-023-01887-y](https://doi.org/10.1038/s41558-023-01887-y)

Published: 04/12/2023

Peer reviewed version

[Cyswllt i'r cyhoeddiad / Link to publication](#)

Dyfyniad o'r fersiwn a gyhoeddwyd / Citation for published version (APA):
Reed, B., Green, M., Jenkins, A., & Gudmundsson, H. (2023). Recent irreversible retreat phase of Pine Island Glacier. *Nature Climate Change*, 14(1), 75-81. <https://doi.org/10.1038/s41558-023-01887-y>

Hawliau Cyffredinol / General rights

Copyright and moral rights for the publications made accessible in the public portal are retained by the authors and/or other copyright owners and it is a condition of accessing publications that users recognise and abide by the legal requirements associated with these rights.

- Users may download and print one copy of any publication from the public portal for the purpose of private study or research.
- You may not further distribute the material or use it for any profit-making activity or commercial gain
- You may freely distribute the URL identifying the publication in the public portal ?

Take down policy

If you believe that this document breaches copyright please contact us providing details, and we will remove access to the work immediately and investigate your claim.

Recent irreversible retreat phase of Pine Island Glacier

Brad Reed^{*1,2}, J. A. Mattias Green¹, Adrian Jenkins², and G. Hilmar Gudmundsson²

¹ School of Ocean Sciences, Bangor University, Menai Bridge, UK

² Department of Geography and Environmental Sciences, Northumbria University, Newcastle, UK

* Corresponding author: brad.reed@northumbria.ac.uk

Abstract

Pine Island Glacier (PIG), a part of the West Antarctic marine ice sheet, has recently undergone substantial changes including speed up, retreat and thinning. Theoretical arguments and modelling work suggest that marine ice sheets can become unstable and undergo irreversible retreat. Here, we use an ice-flow model validated by observational data to show that a rapid PIG retreat in the 1970s from a subglacial ridge to an upstream ice plain was self-enhancing and irreversible. The results suggest that by the early 1970s, the retreat of PIG had reached a point beyond which its original position at the ridge could not be recovered, even during subsequent periods of cooler ocean conditions. The irreversible phase ended by the early 1990s after almost 40 km of retreat and 0.34 mm added to global mean sea level, making PIG the main contributor from the Antarctic Ice Sheet (AIS) in this period.

Introduction

The West Antarctic Ice Sheet (WAIS) has been losing mass since the start of the satellite era¹, and has contributed almost 90% of the overall AIS mass loss since 1992². In the Amundsen Sea Embayment (ASE) in particular, there has been widespread thinning³, accelerated ice flow¹ and grounding-line retreat⁴, which has prompted questions about the future stability of the region^{5,6}. Modelling studies have predicted further retreat under current and future climate conditions^{7–11}, and there is a possibility of a complete collapse of the WAIS if a local destabilisation occurs¹². Due to the retrograde bed (sloping downwards in the inland direction) beneath its largest glaciers, the ASE is vulnerable to a marine ice sheet instability^{13,14}, where a perturbation in grounding-line position could result in irreversible mass loss and grounding-line retreat^{15,16}. The floating extensions of glaciers, known as ice shelves, provide buttressing of upstream grounded ice and can be sufficient to restore stability to unstable grounding-line retreat^{17,18}, particularly through the aid of pinning points such as ice rises and ice rumples^{19,20}. However, ice shelves are susceptible to ocean-induced melting^{21,22}, which can lead to thinning, weakened buttressing and accelerated ice flow^{23,24}.

One of the largest ASE glaciers is Pine Island Glacier (PIG), which has contributed more to global mean sea-level rise in recent decades than any other glacier in Antarctica²⁵. Thinning of the present-day ice shelf and grounding-line retreat can be traced back to the 1940s when an ocean cavity first started to form upstream of a subglacial ridge²⁶. There was further grounding-line retreat and increased ice discharge in the 1970s with the ungrounding of an ice rumples over the highest part of the ridge^{1,27}. These events in the 1940s and 1970s coincide with notable climate anomalies in the central tropical Pacific, which has been shown to have a teleconnection with the Amundsen Sea²⁸. It is possible that tropically forced wind anomalies over the continental shelf break²⁹ caused a shallowing of the thermocline, allowing more warm Circumpolar Deep Water to access the cavity underneath the ice shelf, leading to higher melt and enhanced thinning^{30–33}.

53 Previous ice-flow modelling studies have shown that a shallower thermocline can cause
54 irreversible retreat of an idealised representation of PIG, and this happens when there is
55 a sufficient gap between the subglacial ridge and ice shelf^{34,35}.

56
57 Here, we investigate the retreat of PIG from the ridge and whether the marine ice sheet
58 instability played a role in that retreat. To do this, we use the finite-element, vertically
59 integrated ice-flow model Úa³⁶ to solve the ice dynamics equations in the shallow ice-
60 stream approximation. We first advance a present-day PIG configuration to a steady-state
61 position on the subglacial ridge. This is then perturbed with control forcing that represents
62 mean ocean conditions in the Amundsen Sea. Following this, a warm forced perturbation
63 is applied, which has a shallower thermocline, to represent conditions during a warm
64 period. We use a depth-dependent melt-rate parameterization with a piecewise-linear
65 profile in both scenarios. The final experiment explores the stability regime of the glacier
66 by incrementally changing the basal melting in retreat and advance steady-state
67 simulations.

68 69 **Pre 1940s Pine Island Glacier**

70
71 The model starts from a present-day representation of PIG, with the grounding line of the
72 main central trunk sitting on a 1200 m deep section of bedrock, 47 km upstream of the
73 subglacial ridge crest (Fig. 1). It is then run for 500 years, with no basal melting, allowing
74 a new steady state to be reached. During this period, the ice-stream thickens and advances
75 forward, reduces in speed, and fully grounds on the ridge. Steady state is reached within
76 150 years, with no further change in the central grounding-line position in the remaining
77 350 years of the run (Supplementary Fig. 4). The final ice flux, which is calculated along
78 the present-day grounding-line position (dotted purple in Fig. 1), is 67 Gt yr⁻¹, which is
79 almost within the error range of the earliest observed ice flux, when PIG was still
80 grounded on the ridge¹. It is also similar to the overall surface mass balance of the PIG
81 basin²⁵, showing the glacier is close to a balanced state.

82
83 For the following experiments, we apply a simple depth-dependent melt-rate
84 parameterization, similar to an approach in a previous PIG study⁸. The parameterization
85 represents a two-layer ocean, typically used for conditions in the Amundsen Sea^{35,37}, with
86 zero melting at shallow depths and maximum melting in the deeper areas (Supplementary
87 Fig. 5). Between the two layers is a linearly varying melt rate which represents the ocean
88 thermocline.

89
90 We first run a 100 year simulation with control forcing, which represents average
91 conditions in the Amundsen Sea³⁷. This has a maximum melt rate of 100 m yr⁻¹ below a
92 depth of 700 m^{35,38,39}, decreasing to zero melt at 300 m. The highest melt rate in this
93 model run is at the depth of the ridge crest, hence, much of the ice shelf is initially exposed
94 to high melting (Supplementary Fig. 6).

95
96 At the start of the run, the integrated melt rate across the ice shelf is 144 Gt yr⁻¹, the mean
97 melt rate is 60 m yr⁻¹ and ice flux across the upstream gate (dotted purple in Fig. 1) is 67
98 Gt yr⁻¹. After 100 years, the grounded ice has thinned by an average of 24 m, floating ice
99 has thinned 200-300 m (Fig. 1) and the ice-stream central trunk has sped up by 20 %. The
100 ice shelf rapidly thins in response to the high melting, transforming the profile of the ice-
101 shelf lower surface from convex to concave. The thinning causes grounding-line retreat
102 across the ridge crest, with the slowest retreat occurring from the north end of the ridge,
103 where the bedrock is shallow and wide, and the fastest retreat occurs from the south, along
104 the deep bedrock channel (Fig. 1). Upstream of the grounding line, the thinned grounded
105 ice causes two isolated cavities to form. Despite the grounding line retreating between 5

106 and 20 km, importantly, it remains grounded along the ridge (Fig. 1). By the end of the
107 simulation, the mean melt rate decreases to 18 m yr⁻¹ and the integrated melt rate
108 decreases to 48 Gt yr⁻¹, which agrees with observations of average melt rates beneath
109 PIG^{32,37}. Due to faster flowing ice, the ice flux increases to 79 Gt yr⁻¹, which compares
110 well with the earliest recorded observation¹. The final configuration of the control case is
111 an estimation of how PIG was situated prior to the 1940s.

112 113 **Rapid retreat from a subglacial ridge**

114 Following the control forcing experiment, we simulate the response of PIG to warmer
115 ocean conditions by raising the melt-rate profile by 100 m so that the maximum melt rate
116 is below a depth of 600 m and decreases to zero at 200 m. This is representative of the
117 warmest temperature profiles that were observed in 2009⁴⁰, and this step change in forcing
118 is a similar method to other studies^{8,35,41}. In this experiment the highest melt rate is above
119 the depth of the ridge crest, which compared to the end of the control case results in more
120 than a doubling of the starting mean melt rate (40 m yr⁻¹) and integrated melt rate (120 Gt
121 yr⁻¹) across the ice shelf (Supplementary Fig. 6).

122
123 After 50 years of warm forcing (Fig. 2), there is an average of 25 m further thinning of
124 grounded ice, 100-200 m thinning of floating ice, and a speed up of almost 30 % along
125 the central trunk. During this warm simulation there is a further 10-20 km grounding-line
126 retreat, which, in contrast to the control run, causes an ungrounding from the ridge crest
127 and a new grounding-line position located at the next raised section of bedrock. By the
128 end of the experiment, the mean melt rate decreases to 20 m yr⁻¹ and the integrated melt
129 rate decreases to 74 Gt yr⁻¹. The ice flux at the end of the warm forcing simulation is 96
130 Gt yr⁻¹, which is comparable to the 1996-2000 observations, when PIG was grounded in
131 a similar position¹.

132
133 The temporal changes in total melt and ice fluxes reveal different stages of the retreat
134 during the warm experiment (Fig. 2), similar to a previous idealised study of PIG³⁵.
135 During the first stage, for approximately 8 years, there is a little thinning of floating and
136 grounded ice as the ice shelf experiences higher melt rates. This causes a gradual increase
137 in grounding-line ice flux, a small retreat across the ridge and a decrease in integrated
138 melt rate as the ice shelf thins. During this period, the two isolated cavities start to enlarge
139 and then merge with each other upstream of the ridge, but they remain disconnected from
140 the main outer ice-shelf cavity, so they do not experience any ocean-induced melting.

141
142 The next stage of retreat, between 8-17 years, is illustrated by rapid grounding-line retreat
143 across several areas of retrograde bed (Fig. 2 and Supplementary Figs. 7-8) and the
144 upstream cavities merge with the main outer cavity via the deep southern channel. This
145 creates an ice rumple over the ridge in the North, and then the ice shelf ungrounds
146 completely around 17 years. This stage of retreat is illustrated by a sharp increase in
147 integrated melt rate as the grounding line enters a deeper section of the bedrock and
148 experiences higher melting, causing a notable increase in grounding-line ice flux.

149
150 For the final retreat stage, from 18 years until the end of the simulation, there is gradual
151 grounding-line retreat onto the next prominent section of bedrock, and a slow decrease in
152 integrated melt rate and ice flux as the ice shelf continues to thin (Fig. 2). The final
153 grounding-line position, melt rate and ice fluxes all approach their steady-state values as
154 the ice stream stabilizes in its new upstream position.

155
156
157
158

Hysteresis behaviour of Pine Island Glacier

160

161

162

163

164

165

166

167

168

169

170

171

172

To assess whether the warm forced retreat is reversible we perform a reversibility analysis, which consists of 38 separate steady-state simulations, with 19 comprising a retreat group and 19 a subsequent advance group. The retreat simulations all start from the no-melt steady-state solution at the ridge, approximately 47 km downstream of the present-day grounding line (Fig. 1). The advance simulations all start from the final steady-state solution of the last model run in the retreat group, which is approximately 11 km from the present-day grounding line. All model simulations in the two groups have a different thermocline depth in the melt forcing, which ranges from 1300 m to 400 m (Fig. 3), and each is run to a steady state, which indicates how far the grounding line can move under each forcing.

173

174

175

176

177

178

179

180

181

182

The first six retreat simulations, with thermocline depths between 1300 m and 1050 m, do not cause any thinning of the ice shelf because the highest melt rates are deeper than the ridge crest and lower ice surface. As the thermocline is raised above 1050 m, the steady-state solutions show a gradual, continual thinning of the ice shelf and migration of the grounding line from the front of the ridge to the back (Fig. 3). Once the thermocline is raised above 700 m, the steady-state grounding-line retreats a further 20 km from the ridge crest to the next prominent high point in the bed. For thermocline depths above 650 m there is only a further 5 km of retreat, with the final steady-state grounding line stabilizing on the upstream ice plain.

183

184

185

186

187

188

189

190

191

192

193

194

The large migration in grounding-line position in response to the small change in thermocline depth above 700 m shows that the grounding line is highly sensitive to changes in the melt forcing but does not necessarily mean a stability threshold has been crossed. Therefore, we reverse the forcing to explore the response of the grounding line. As the thermocline is lowered from a depth of 400 m to 1000 m, there is a gradual thickening of the ice shelf and 8 km grounding-line advance from the upstream bed rise. The thermocline must be lowered below 1000 m for the melt rates to become small enough to allow for sufficient thickening of the ice shelf and regrounding on the ridge. There is no change in ice-shelf thickness or grounding line once the thermocline is lowered beneath a depth of 1050 m and the steady-state position coincides with the original starting position, 47 km from the present-day grounding line.

195

196

197

198

199

200

201

202

203

204

205

206

207

208

209

210

It is evident from this experiment that a hysteretic behaviour exists when PIG is forced with a changing thermocline depth in the melt forcing. There are multiple steady states for the same forcing, whereby the final grounding-line position depends on the history of forcing applied, whether the glacier has been retreating or advancing. The stable steady-state positions are generally situated on the prograde slopes of the ridge and ice plain, and unstable regions on the large retrograde sections (Fig. 3 and Supplementary Figs. 9-10). However, this does not hold everywhere as there are some local differences, which are possibly due to ice shelf buttressing³⁶. Hence, we cannot make a general statement about bed slope and ice sheet stability as can be done for the one-dimensional example^{13,14}. There are two threshold thermocline depths at 700 m and 1000 m, that when crossed, lead to irreversible grounding-line motion. These are irreversible transitions because the thermocline depth must be changed more than the reverse forcing to achieve the same grounding-line position. These results imply that PIG experienced a marine ice sheet instability retreat as it began to lose contact with the subglacial ridge after the 1940s climate anomaly.

211 Additional experiments were also carried out to test the dependency of our results on the
212 selected model parameters and the choice of bedrock state. The first experiment used a
213 smaller slipperiness coefficient in the Weertman sliding law (equation (7)) to account for
214 a different sediment profile beneath the glacier⁴². The second experiment used a modified
215 power law for the basal traction (equation (8)), which has been shown to affect grounding-
216 line retreat and the rate of mass loss⁴³⁻⁴⁵. The third experiment was run on a lower bed to
217 test the impact of solid-earth feedbacks. For this simulation the bed was lowered by 10 m
218 at the start of the run, where we had assumed a high uplift rate of 20 cm yr⁻¹ for our entire
219 model period⁴⁶. The final experiment used a different melt-rate parameterization, which
220 has been used in a previous model intercomparison project for an idealized representation
221 of the main trunk of PIG⁴⁷. In all four experiments a hysteresis was present in response
222 to the changing thermocline depth in the melt forcing (Supplementary Figs. 11-14).

227 Discussion

228
229 Prior to the 1940s, it is likely that PIG had been grounded in a stable position on a
230 subglacial ridge 47 km downstream from its present-day position²⁶. Then, following
231 notable climate anomalies, and probably warmer basal conditions, in the 1940s and
232 1970s^{32,48}, a pre-existing cavity beneath the ice shelf became connected with the open
233 ocean and the glacier started to retreat from the ridge crest^{26,27}. In the subsequent decades,
234 PIG failed to recover its original position on the ridge, despite periods of cool ocean
235 conditions which should have caused less melting and more thickening³². A decadal
236 variability in local ocean conditions, largely driven by changes in the tropical Pacific
237 Ocean³², is not reflected in the near monotonic increase in ice discharge that has been
238 observed since the start of the satellite period in the 1970s¹. By the early 1990s, the PIG
239 grounding line had completely retreated off the ridge, across the retrograde bed,
240 stabilizing at an ice plain 30 km upstream⁴⁹ (Supplementary Fig. 15). This raises the
241 question of whether its retreat from the ridge was an induced instability in response to the
242 initial perturbation.

243
244 Using a vertically integrated ice-flow model and a depth-dependent melt-rate
245 parameterization, we investigated the aspect of the retreat from the subglacial ridge that
246 was due to internal dynamics of the system rather than changes in external forcing. The
247 ocean forcing in this experiment is therefore simplified as we focus solely on whether the
248 marine ice sheet instability played a role in the retreat of PIG from the ridge. Prior to the
249 control simulation, the grounding line is in a stable position at the ridge crest. When basal
250 melting is applied, to represent average ocean conditions in Amundsen Sea, the ice stream
251 thins and the grounding line retreats, but it remains grounded on the ridge. Therefore,
252 prior to the 1940s, PIG probably experienced temporary periods of migration back and
253 forth on the ridge in response to variable ocean conditions³².

254
255 When higher melt rates are applied for an extended period of time, to represent what may
256 have happened during the 1940s El Niño event^{26,32}, there is a rapid retreat down the
257 retrograde slope facilitated by the merging of upstream cavities. Although we used a
258 simple melt-rate parameterization, the initial behaviour of retreat, the speed at which it
259 progresses and the final ungrounding of a pinning point above the ridge are all comparable
260 with satellite observations and sediment records from the 1940s and 1970s^{26,27}.

261
262 Our stability analysis suggests that by the early 1970s, when PIG had already started
263 retreating from the ridge²⁷, a threshold had been crossed, whereby its previous position

264 could not be restored during subsequent cooler periods³². This irreversible phase came to
265 a halt as the grounding line reached a new steady state on the next bed high point (Fig.
266 3). This location coincides with its early 1990s position, when PIG was grounded at an
267 ice plain and had experienced a decrease in grounding-line ice flux^{1,49,50}. During the
268 suspected period of rapid retreat from the 1970s to the early 1990s, PIG was responsible
269 for a third of the mass loss from West Antarctica, and almost 13 % of the overall Antarctic
270 Ice Sheet mass loss²⁵. Despite its basin comprising of only 1.5 % of the entire ice sheet
271 area, PIG was the largest contributor to sea-level rise during those years, adding 0.34 mm
272 in total²⁵.

273
274 Climate change is likely to cause further upstream migration of grounding lines of WAIS.
275 In the Amundsen Sea, as local wind trends change in response to internal and external
276 forcing^{29,51}, this may deliver more warm water to the continental shelf^{30,31}, leading to
277 increased basal melt⁵² and ice-shelf thinning. Previous modelling studies of the behaviour
278 of Amundsen Sea glaciers have suggested the existence of multiple stability thresholds,
279 which when crossed lead to irreversible mass loss at some point in the future^{9,16}. This
280 marine ice sheet instability is theoretically well understood^{13,14}, and robustly replicated in
281 numerical models^{8,9,16,53}, however, the hypothesis has hitherto had little direct
282 observational support. This is in part due to the long timescales involved and the sparsity
283 of relevant observations.

284
285 Here, we have now shown that the recent observed grounding-line retreat of PIG, in the
286 period from the 1940s to 1990s, was irreversible and thereby provided an observational
287 validated example of the marine ice sheet instability. Our ice-flow model is based on the
288 same physical assumptions used in previous future simulations^{9,16} and therefore this
289 greatly strengthens our confidence in the capability of ice sheet models and their ability
290 to simulate and predict highly nonlinear behaviours of large ice sheets. Furthermore, the
291 results presented here are robust and insensitive to our choice of model parameters. These
292 simulations suggest that the recent retreat phase of PIG may have been primarily
293 internally driven, as opposed to external forced. While ocean-induced melt may have been
294 the initial trigger, the retreat phase was driven by internal ice-dynamical processes leading
295 to irrevocable loss of ice that could not be recovered by a reversal in external climatic
296 condition. The implications for the future are clear: What has happened in the recent past,
297 can happen again and, as predicted by ice-flow models, future ice loss from the WAIS
298 may become self-sustaining, amplified and irreversible as the ice sheets enter unstable
299 phases of retreat.

300 301 **Acknowledgments**

302
303 The authors acknowledge the support and resources of the Supercomputing Wales project,
304 which is part-funded by the European Regional Development Fund (ERDF) via Welsh
305 Government. BR was supported by the ENVISION Doctoral Training Partnership
306 studentship from the Natural Environment Research Council and was in part supported
307 by UKRI (grant number MR/W011816/1). GHG and AJ have received funding from the
308 European Union's Horizon 2020 research and innovation programme under grant
309 agreement no. 820575: Tipping Points in the Antarctic Climate Components.

310 311 **Author contributions**

312
313 BR designed and carried out all model simulations and analysed the results. GHG assisted
314 with experiment design. BR wrote the manuscript and all authors assisted with the
315 conception of the study and provided feedback and comments during editing.

316

317

Competing interests

318

There are no competing interests.

319

320

321

Figure captions

322

323

Fig. 1. Pine Island Glacier subjected to different basal melt forcing. **a, b,** Bedrock elevation with overlain grounding lines (**a**) and flowline profiles (**b**) for the initial model setup, control and warm simulations. The flowline position is shown in dashed cyan in **a**. In both panels, the present-day geometry is shown in dotted purple and the steady-state geometry after no basal melting for 500 years is shown in dash-dotted purple. The black solid line shows the geometry after 100 years of control forcing, with a 700 m thermocline depth, and the red solid line shows the geometry following another 50 years of warm forcing, with a 600 m thermocline. The zero position along the flowline in **b** corresponds to the present-day grounding-line position.

324

325

326

327

328

329

330

331

332

Fig. 2. Warm forced retreat of Pine Island Glacier. **a, b,** Bedrock elevation with overlain grounding lines (**a**) and flowline profiles (**b**) during the warm forcing experiment. The zero position along the flowline in **b** corresponds to the present-day grounding line. **c,** Grounding-line position during the model simulation along the dashed cyan flowline which is shown in **a**. **d, e** Total integrated melt rate over the entire ice shelf (**d**) and grounding-line flux and calving flux (**e**) during the experiment. The grounding-line flux is calculated along the present-day grounding-line position (dotted purple in Fig. 1) for all timesteps. The colour of grounding lines, profiles and plot markers in all panels show the model year during the experiment (increment of 2 years). Shaded and unshaded regions in **c-e** indicate the different stages of retreat. Open markers in **c, d** and **e** show the steady-state grounding-line position, integrated melt rate and ice fluxes, respectively.

333

334

335

336

337

338

339

340

341

342

343

344

Fig. 3. Reversibility experiments. **a-d,** Final steady-state grounding lines (**a, c**) and flowline profiles (**b, d**) for model simulations with different thermocline depths. **e,** Flowline grounding-line position as a function of thermocline depth for each model simulation. Upward pointing triangles indicate the final grounding-line position for simulations which start at the subglacial ridge in the retreat group. Downward pointing triangles indicate the final grounding-line position for simulations which start at the upstream ice plain position in the advance group. The advance simulations all start from the final grounding-line position from the last retreat simulation (11 km along flowline). The open black and red triangles indicate the grounding-line position from the control (700 m) and warm (600 m) transient experiments, respectively, that were shown in Fig. 1. Note the solid black lines between markers in **e** are not results of model runs but are for visual purposes only. The grey shaded region in **e** corresponds to steep retrograde sections of bed, which are also indicated by black dash-dotted lines in all panels. The location of the flowline is shown as a dash-dotted line in **a** and **c**.

345

346

347

348

349

350

351

352

353

354

355

356

357

358

359

360

References

361

362

1. Mouginot, J., Rignot, E. & Scheuchl, B. Sustained increase in ice discharge from the Amundsen Sea Embayment, West Antarctica, from 1973 to 2013. *Geophysical Research Letters* **41**, 1576–1584 (2014).

363

364

365

366

2. Shepherd, A. *et al.* Mass balance of the Antarctic Ice Sheet from 1992 to 2017. *Nature* **558**, 219–222 (2018).

365

366

- 367 3. Konrad, H. *et al.* Uneven onset and pace of ice-dynamical imbalance in the
368 Amundsen Sea Embayment, West Antarctica. *Geophysical Research Letters* **44**, 910–
369 918 (2017).
- 370 4. Rignot, E., Mouginot, J., Morlighem, M., Seroussi, H. & Scheuchl, B. Widespread,
371 rapid grounding line retreat of Pine Island, Thwaites, Smith, and Kohler glaciers, West
372 Antarctica, from 1992 to 2011. *Geophysical Research Letters* **41**, 3502–3509 (2014).
- 373 5. Urruty, B. *et al.* The stability of present-day Antarctic grounding lines — Part A : No
374 indication of marine ice sheet instability in the current geometry. 1–34 (2022).
- 375 6. Reese, R. *et al.* The stability of present-day Antarctic grounding lines — Part B :
376 Possible commitment of regional collapse under current climate. *The Cryosphere*
377 *Discussions* (2022).
- 378 7. Joughin, I., Smith, B. E. & Holland, D. M. Sensitivity of 21st century sea level to
379 ocean-induced thinning of Pine Island Glacier, Antarctica. *Geophysical Research*
380 *Letters* **37**, n/a-n/a (2010).
- 381 8. Favier, L. *et al.* Retreat of Pine Island Glacier controlled by marine ice-sheet
382 instability. *Nature Climate Change* **4**, 117–121 (2014).
- 383 9. Joughin, I., Smith, B. E. & Medley, B. Marine ice sheet collapse potentially under
384 way for the Thwaites Glacier Basin, West Antarctica. *Science* **344**, 735–738 (2014).
- 385 10. Seroussi, H. *et al.* Continued retreat of Thwaites Glacier, West Antarctica,
386 controlled by bed topography and ocean circulation. *Geophysical Research Letters* **44**,
387 6191–6199 (2017).
- 388 11. Cornford, S. L. *et al.* Century-scale simulations of the response of the West
389 Antarctic Ice Sheet to a warming climate. *The Cryosphere* **9**, 1579–1600 (2015).
- 390 12. Feldmann, J. & Levermann, A. Collapse of the West Antarctic Ice Sheet after
391 local destabilization of the Amundsen Basin. *Proceedings of the National Academy of*
392 *Sciences* **112**, 14191–14196 (2015).
- 393 13. Weertman, J. Stability of the junction of an ice sheet and an ice shelf. *Journal*
394 *of Glaciology* **13**, 3–11 (1974).
- 395 14. Schoof, C. Ice sheet grounding line dynamics: Steady states, stability, and
396 hysteresis. *Journal of Geophysical Research: Earth Surface* **112**, (2007).
- 397 15. Garbe, J., Albrecht, T., Levermann, A., Donges, J. F. & Winkelmann, R. The
398 hysteresis of the Antarctic Ice Sheet. *Nature* **585**, 538–544 (2020).
- 399 16. Rosier, S. H. R. *et al.* The tipping points and early warning indicators for
400 Pine Island Glacier, West Antarctica. *Cryosphere* **15**, 1501–1516 (2021).
- 401 17. Gudmundsson, G. H. Ice-shelf buttressing and the stability of marine ice
402 sheets. *The Cryosphere* **7**, 647–655 (2013).
- 403 18. Pegler, S. S. Suppression of marine ice sheet instability. *J. Fluid Mech* **857**,
404 648–680 (2018).
- 405 19. Schlegel, N. J. *et al.* Exploration of Antarctic Ice Sheet 100-year contribution
406 to sea level rise and associated model uncertainties using the ISSM framework.
407 *Cryosphere* **12**, 3511–3534 (2018).

- 408 20. Favier, L., Pattyn, F., Berger, S. & Drews, R. Dynamic influence of pinning
409 points on marine ice-sheet stability: A numerical study in Dronning Maud Land, East
410 Antarctica. *Cryosphere* **10**, 2623–2635 (2016).
- 411 21. Payne, A. J., Vieli, A., Shepherd, A. P., Wingham, D. J. & Rignot, E. Recent
412 dramatic thinning of largest West Antarctic ice stream triggered by oceans. *Geophysical*
413 *Research Letters* **31**, 1–4 (2004).
- 414 22. Pritchard, H. *et al.* Antarctic ice-sheet loss driven by basal melting of ice
415 shelves. *Nature* **484**, 502–505 (2012).
- 416 23. Gudmundsson, G. H., Paolo, F. S., Adusumilli, S. & Fricker, H. A.
417 Instantaneous Antarctic ice sheet mass loss driven by thinning ice shelves. *Geophysical*
418 *Research Letters* **46**, 13903–13909 (2019).
- 419 24. Joughin, I., Shapero, D., Dutrieux, P. & Smith, B. Ocean-induced melt
420 volume directly paces ice loss from Pine Island Glacier. *Science Advances* **7**, (2021).
- 421 25. Rignot, E. *et al.* Four decades of Antarctic Ice Sheet mass balance from
422 1979–2017. *Proceedings of the National Academy of Sciences* **116**, 1095–1103 (2019).
- 423 26. Smith, J. A. *et al.* Sub-ice-shelf sediments record history of twentieth-century
424 retreat of Pine Island Glacier. *Nature* **541**, 77–80 (2017).
- 425 27. Jenkins, A. *et al.* Observations beneath Pine Island Glacier in West-
426 Antarctica and implications for its retreat. *Nature Geoscience* **3**, 468–472 (2010).
- 427 28. Lachlan-Cope, T. & Connolley, W. Teleconnections between the tropical
428 Pacific and the Amundsen-Bellinghausens Sea: Role of the El Niño/Southern
429 Oscillation. *Journal of Geophysical Research Atmospheres* **111**, (2006).
- 430 29. Holland, P. R., Bracegirdle, T. J., Dutrieux, P., Jenkins, A. & Steig, E. J.
431 West Antarctic ice loss influenced by internal climate variability and anthropogenic
432 forcing. *Nature Geoscience* **12**, 718–724 (2019).
- 433 30. Thoma, M., Jenkins, A., Holland, D. & Jacobs, S. Modelling Circumpolar
434 Deep Water intrusions on the Amundsen Sea continental shelf, Antarctica. *Geophysical*
435 *Research Letters* **35**, 2–7 (2008).
- 436 31. Steig, E. J., Ding, Q., Battisti, D. S. & Jenkins, A. Tropical forcing of
437 circumpolar deep water inflow and outlet glacier thinning in the amundsen sea
438 embayment, west antarctica. *Annals of Glaciology* **53**, 19–28 (2012).
- 439 32. Jenkins, A. *et al.* Decadal ocean forcing and Antarctic Ice Sheet response:
440 Lessons from the Amundsen Sea. *Oceanography* **29**, 106–117 (2016).
- 441 33. Naughten, K. A. *et al.* Simulated Twentieth-Century Ocean Warming in the
442 Amundsen Sea, West Antarctica. *Geophysical Research Letters* **49**, (2022).
- 443 34. De Rydt, J., Holland, P. R., Dutrieux, P. & Jenkins, A. Geometric and
444 oceanographic controls on melting beneath Pine Island Glacier. *Journal of Geophysical*
445 *Research: Oceans* **119**, 2420–2438 (2014).
- 446 35. De Rydt, J. & Gudmundsson, G. H. Coupled ice shelf-ocean modeling and
447 complex grounding line retreat from a seabed ridge. *Journal of Geophysical Research*
448 *F: Earth Surface* **121**, 865–880 (2016).

- 449 36. Gudmundsson, G. H., Krug, J., Durand, G., Favier, L. & Gagliardini, O. The
450 stability of grounding lines on retrograde slopes. *The Cryosphere* **6**, 1497–1505 (2012).
- 451 37. Dutrieux, P. *et al.* Strong sensitivity of Pine Island ice-shelf melting to
452 climatic variability. *Science* **343**, 174–178 (2014).
- 453 38. Dutrieux, P. *et al.* Pine Island glacier ice shelf melt distributed at kilometre
454 scales. *Cryosphere* **7**, 1543–1555 (2013).
- 455 39. Bindschadler, R., Vaughan, D. G. & Vornberger, P. Variability of basal melt
456 beneath the Pine Island Glacier ice shelf, West Antarctica. *Journal of Glaciology* **57**,
457 581–595 (2011).
- 458 40. Jacobs, S. S., Jenkins, A., Giulivi, C. F. & Dutrieux, P. Stronger ocean
459 circulation and increased melting under Pine Island Glacier ice shelf. *Nature*
460 *Geoscience* **4**, 519–523 (2011).
- 461 41. Bradley, A. T., Bett, D. T., Dutrieux, P., De Rydt, J. & Holland, P. R. The
462 Influence of Pine Island Ice Shelf Calving on Basal Melting. *Journal of Geophysical*
463 *Research: Oceans* **127**, e2022JC018621 (2022).
- 464 42. Muto, A. *et al.* Subglacial bathymetry and sediment distribution beneath Pine
465 Island Glacier ice shelf modeled using aerogravity and in situ geophysical data: New
466 results. *Earth and Planetary Science Letters* **433**, 63–75 (2016).
- 467 43. Yu, H., Rignot, E., Seroussi, H. & Morlighem, M. Retreat of Thwaites
468 Glacier, West Antarctica, over the next 100 years using various ice flow models, ice
469 shelf melt scenarios and basal friction laws. *The Cryosphere* **12**, 3861–3876 (2018).
- 470 44. Brondex, J., Gagliardini, O., Gillet-Chaulet, F. & Durand, G. Sensitivity of
471 grounding line dynamics to the choice of the friction law. *Journal of Glaciology* **63**,
472 854–866 (2017).
- 473 45. Brondex, J., Gillet-Chaulet, F. & Gagliardini, O. Sensitivity of centennial
474 mass loss projections of the Amundsen basin to the friction law. *The Cryosphere* **13**,
475 177–195 (2019).
- 476 46. Barletta, V. R. *et al.* Observed rapid bedrock uplift in Amundsen Sea
477 Embayment promotes ice-sheet stability. *Science* **360**, 1335–1339 (2018).
- 478 47. Asay-Davis, X. S. *et al.* Experimental design for three interrelated marine ice
479 sheet and ocean model intercomparison projects: MISMIP v. 3 (MISMIP+), ISOMIP v.
480 2 (ISOMIP+) and MISOMIP v. 1 (MISOMIP1). *Geosci. Model Dev* **9**, 2471–2497
481 (2016).
- 482 48. Jenkins, A. *et al.* West Antarctic Ice Sheet retreat in the Amundsen Sea
483 driven by decadal oceanic variability. *Nature Geoscience* **11**, 733–738 (2018).
- 484 49. Park, J. W. *et al.* Sustained retreat of the Pine Island Glacier. *Geophysical*
485 *Research Letters* **40**, 2137–2142 (2013).
- 486 50. Corr, H. F. J., Doake, C. S. M., Jenkins, A. & Vaughan, D. G. Investigations
487 of an ‘ice plain’ in the mouth of Pine Island Glacier, Antarctica. *Journal of Glaciology*
488 **47**, 51–57 (2001).

- 489 51. Holland, P. R. *et al.* Anthropogenic and internal drivers of wind changes over
 490 the Amundsen Sea, West Antarctica, during the 20th and 21st centuries. *The*
 491 *Cryosphere* **16**, 5085–5105 (2022).
- 492 52. Jourdain, N. C., Mathiot, P., Burgard, C., Caillet, J. & Kittel, C. Ice Shelf
 493 Basal Melt Rates in the Amundsen Sea at the End of the 21st Century. *Geophysical*
 494 *Research Letters* **49**, e2022GL100629 (2022).
- 495 53. Pattyn, F. *et al.* Results of the marine ice sheet model intercomparison
 496 project, MISIP. *Cryosphere* **6**, 573–588 (2012).

497

498 **Methods**

499

500 **Ice-flow model**

501

502 In this study we used the finite-element, vertically integrated ice-flow model $\dot{U}a^{36,54}$ to
 503 solve the ice dynamics equations in the shallow ice-stream approximation (SSTREAM or
 504 SSA)⁵⁵. The model has previously been used to study tipping points and drivers of retreat
 505 of Pine Island Glacier^{16,56}, grounding-line stability and ice-shelf buttressing^{36,57,58} and in
 506 a number of intercomparison projects^{59–61}.

507

508 The vertically integrated, or two horizontal dimension, momentum equations can be
 509 written in compact form as

$$\nabla_{xy} \cdot (hR) - t_{bh} = \rho_i g h \nabla_{xy} s + \frac{1}{2} g h^2 \nabla_{xy} \rho_i \quad (1)$$

510

511 where h is the ice thickness, t_{bh} is the horizontal component of the bed-tangential basal
 512 traction t_b , ρ_i is the vertically averaged ice density, g is gravitational acceleration, s is the
 513 ice upper surface elevation, and R is the resistive stress tensor defined as

514

$$R = \begin{pmatrix} 2\tau_{xx} + \tau_{yy} & \tau_{xy} \\ \tau_{xy} & 2\tau_{yy} + \tau_{xx} \end{pmatrix} \quad (2)$$

515

516 and

517

$$\nabla_{xy} = (\partial_x, \partial_y)^T. \quad (3)$$

518 Here, τ_{ij} are the components of the deviatoric stress tensor. The relationship between
 519 deviatoric stresses τ_{ij} and strain-rates ϵ_{ij} is given by Glen's flow law

520

$$\dot{\epsilon}_{ij} = A \tau^{n-1} \tau_{ij}, \quad (4)$$

521

522 where τ is the second invariant of the deviatoric stress tensor

523

$$\tau = \sqrt{\tau_{ij} \tau_{ij} / 2}, \quad (5)$$

524

525 A is a spatially varying ice rate factor determined using inverse methods and $n = 3$ is a
 526 creep exponent. In our main set of experiments the basal traction is given by Weertman's
 527 sliding law

528

$$t_b = G\beta^2 v_b, \quad (6)$$

where G is a floating mask, with $G = 1$ for grounded ice and $G = 0$ otherwise and v_b is the horizontal component of the bed-tangential ice-velocity. In equation (6), β^2 is given by

$$\beta^2 = C^{-1/m} |v_b|^{1/m-1}, \quad (7)$$

where C is a spatially varying slipperiness coefficient, determined using inverse methods, and $m = 3$ which gives a non-linear viscous relationship. Downstream of the grounding line the slipperiness coefficient is set to a constant of $C = 0.03 \text{ m yr}^{-1} \text{ kPa}^{-3}$, which allows the ice stream to advance forward. This constant is representative of upstream slipperiness values along the fast-flowing tributaries.

In two additional experiments, a different basal sliding setup was used. Firstly, a downstream slipperiness coefficient of $C = 0.01 \text{ m yr}^{-1} \text{ kPa}^{-3}$, representing a ‘stickier’ bed, was tested. Whilst in the second experiment, a modified power law was used for the basal traction⁴⁷. This is given by

$$t_b = \frac{G\beta^2 |v_b| \mu_k N}{((\mu_k N)^m + (G\beta^2 |v_b|)^m)^{1/m}} \frac{v_b}{|v_b|} \quad (8)$$

where μ_k is the coefficient of kinetic friction and is set to $\mu_k = 0.5$.

Model domain and mesh

The model domain includes the grounded catchment of PIG (182,000 km²) and its floating ice shelf⁶² (Supplementary Fig. 1). The calving front is fixed throughout the study and corresponds approximately to the 2008/09 ice front, which is not far from its 1940s position^{63,64}. For all experiments in this study, a Dirichlet boundary condition is imposed on the grounded portion of the boundary to set the velocity to zero along the ice divides, and a Neumann boundary condition arising from ocean pressure is imposed along the ice front.

An irregular, triangular mesh was generated using MESH2D⁶⁵ for the entire domain, and consisted of 58777 linear elements and 29797 nodes. The mesh was refined for ice-shelf elements (1 km) and in areas of high strain rate and high strain rate gradients (0.7-1.5 km), whereas larger elements (10 km) were used for the slowest moving ice inland away from the main tributaries (Supplementary Fig. 2). This gave a mesh with minimum, median, and maximum element sizes of 563 m, 1311 m and 11330 m respectively. For the control and warm experiments, a further grounding-line mesh adaption was applied to ensure fine element sizes were used in a crucial transition area. Due to computational and time limitations, no mesh adaption was used for the reversibility experiments.

Input data

This study aims to simulate the response of a 1940s PIG to a change in external forcing, however, with very little data available for that period we set up our model using present day observations and then let the model evolve in time to get an approximate

576 configuration for 1940. The bedrock topography, ice thickness, surface elevation and ice
577 density were taken from BedMachine Antarctica, v2⁶⁶. These datasets have a resolution
578 of 500 m and nominal data of 2015. Some local adjustments were made to the ice-shelf
579 thickness near the grounding line to ensure the hydrostatic floating condition was met. As
580 the BedMachine data represents a recent bed geometry, we also ran an additional
581 experiment with a lower bed to test the impact of solid-earth feedbacks. The upper surface
582 accumulation was from given by the RACMO2.3p2 dataset⁶⁷ and was averaged between
583 1979 to 2016.

584 **Inversion**

585
586
587 To initialise the model, we used present day velocities from the MEaSURES Annual
588 Antarctic Ice Velocity Maps^{68,69} dataset to invert for the slipperiness parameter and the
589 ice rate factor (Supplementary Fig. 3). For the inversion process, Úa minimises a cost
590 function containing a misfit and a regularisation term, using the adjoint method and
591 Tikhonov regularisation, as has been done in previous studies^{70–72}.

592 **Melt-rate parameterization**

593
594
595 The basal melt rate is given by a depth dependent parameterization (Supplementary Figs.
596 5 and 6), similar to a previous study on Pine Island Glacier retreat⁸. Although this is a
597 simple parameterization, it allows for conclusions to be made about the direct effect of
598 basal melting. We also repeated our stability analysis using a different melt-rate
599 parameterization which has been used in a previous model intercomparison project⁴⁷. To
600 ensure the grounding-line retreat was not overestimated, we applied basal melting on
601 mesh elements that are strictly downstream of the grounding line⁷³. For the stability
602 analysis, model simulations were run for 100s of years until a steady state was reached.
603 During these runs, to avoid unrealistic retreat along the southwest tributary, close to the
604 model domain boundary, the basal melting was set to zero for elements in this region.

605 **Data availability**

606
607
608
609 Model data inputs that are required to reproduce the experiments in this study are freely
610 available together with all of the main experiment outputs on Zenodo at
611 <https://doi.org/10.5281/zenodo.10043471> (ref. ⁷⁴).

612 **Code availability**

613
614
615 The experiments presented here were performed using the ice-flow model Úa, which is
616 publicly accessible^{36,54} and the version used in this study is available at
617 <https://github.com/GHilmarG/UaSource/commit/a3133bf>. The code to reproduce the
618 figures in this study is available on Zenodo at <https://doi.org/10.5281/zenodo.10043471>
619 (ref. ⁷⁴).

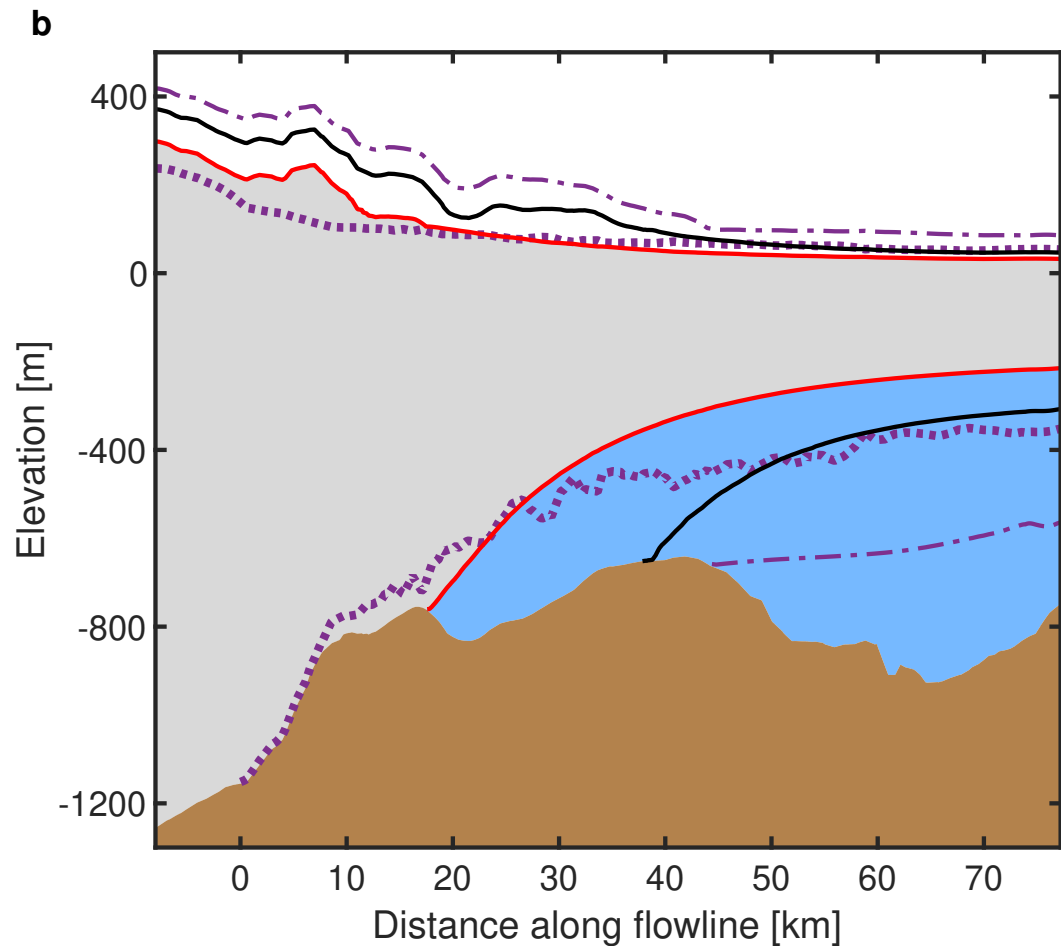
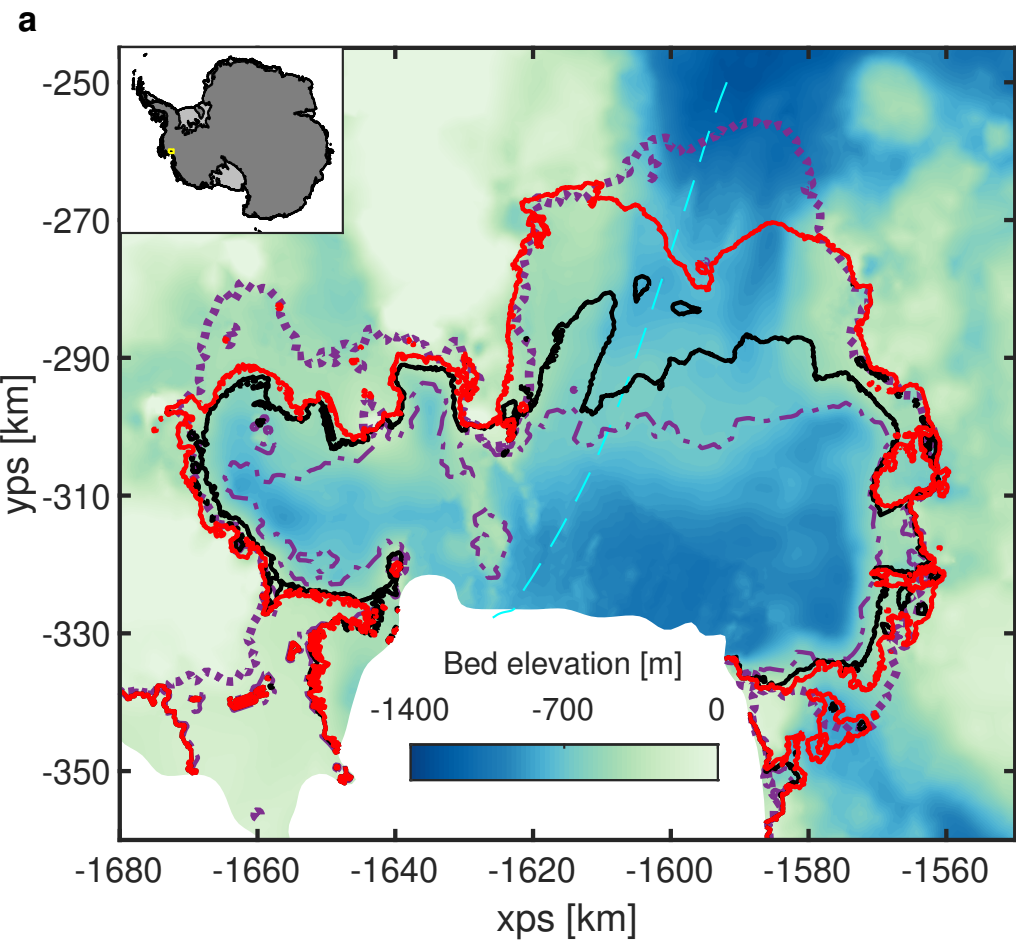
620 **Methods-only references**

- 621
622
623 54. Gudmundsson, G. H. GHilmarG/UaSource: Ua2019b. Zenodo
624 <https://doi.org/10.5281/zenodo.3706624> (2020).

- 625 55. Macayeal, D. R. Large-scale ice flow over a viscous basal sediment: theory and
626 application to ice stream B, Antarctica. *Journal of Geophysical Research* **94**, 4071–4087
627 (1989).
- 628 56. De Rydt, J., Reese, R., Paolo, F. S. & Hilmar Gudmundsson, G. Drivers of Pine
629 Island Glacier speed-up between 1996 and 2016. *Cryosphere* **15**, 113–132 (2021).
- 630 57. Reese, R., Gudmundsson, G. H., Levermann, A. & Winkelmann, R. The far reach of
631 ice-shelf thinning in Antarctica. *Nature Climate Change* **8**, 53–57 (2018).
- 632 58. Hill, E. A., Hilmar Gudmundsson, G., Rachel Carr, J. & Stokes, C. R. Velocity
633 response of Petermann Glacier, northwest Greenland, to past and future calving events.
634 *Cryosphere* **12**, 3907–3921 (2018).
- 635 59. Cornford, S. L. *et al.* Results of the third Marine Ice Sheet Model Intercomparison
636 Project (MISMIP+). *Cryosphere* **14**, 2283–2301 (2020).
- 637 60. Levermann, A. *et al.* Projecting Antarctica’s contribution to future sea level rise from
638 basal ice shelf melt using linear response functions of 16 ice sheet models (LARMIP-2).
639 *Earth System Dynamics* **11**, 35–76 (2020).
- 640 61. Pattyn, F. *et al.* Grounding-line migration in plan-view marine ice-sheet models:
641 Results of the ice2sea MISMIP3d intercomparison. *Journal of Glaciology* **59**, 410–422
642 (2013).
- 643 62. Rignot, E., Jacobs, S., Mouginot, J. & Scheuchl, B. Ice-shelf melting around
644 antarctica. *Science* **341**, 266–270 (2013).
- 645 63. Rignot, E. Ice-shelf changes in Pine Island Bay, Antarctica, 1947–2000. *Journal of*
646 *Glaciology* **48**, 247–256 (2002).
- 647 64. Arndt, J. E. *et al.* Bathymetric controls on calving processes at Pine Island Glacier.
648 *Cryosphere* **12**, 2039–2050 (2018).
- 649 65. Engwirda, D. Locally optimal Delaunay-refinement and optimisation-based mesh
650 generation. (2014).
- 651 66. Morlighem, M. *et al.* Deep glacial troughs and stabilizing ridges unveiled beneath
652 the margins of the Antarctic ice sheet. *Nature Geoscience* **13**, 132–137 (2020).
- 653 67. Melchior Van Wessem, J. *et al.* Modelling the climate and surface mass balance of
654 polar ice sheets using RACMO2 - Part 2: Antarctica (1979–2016). *Cryosphere* **12**, 1479–
655 1498 (2018).
- 656 68. Mouginot, J., Rignot, E., Scheuchl, B. & Millan, R. Comprehensive Annual Ice
657 Sheet Velocity Mapping Using Landsat-8, Sentinel-1, and RADARSAT-2 Data. *Remote*
658 *Sensing 2017, Vol. 9, Page 364* **9**, 364 (2017).
- 659 69. Mouginot, J., Rignot, E. & Scheuchl, B. MEaSURES Annual Antarctic Ice Velocity
660 Maps, Version 1. (2017) doi:10.5067/9T4EPQXTJYW9.
- 661 70. Mitcham, T., Gudmundsson, G. H. & Bamber, J. L. The instantaneous impact of
662 calving and thinning on the Larsen C Ice Shelf. *The Cryosphere* **16**, 883–901 (2022).
- 663 71. Hill, E. A., Gudmundsson, G. H., Carr, J. R., Stokes, C. R. & King, H. M. Twenty-
664 first century response of Petermann Glacier, northwest Greenland to ice shelf loss. *Journal*
665 *of Glaciology* **67**, 147–157 (2021).

- 666 72. Reese, R., Winkelmann, R. & Hilmar Gudmundsson, G. Grounding-line flux formula
667 applied as a flux condition in numerical simulations fails for buttressed Antarctic ice
668 streams. *Cryosphere* **12**, 3229–3242 (2018).
- 669 73. Seroussi, H. & Morlighem, M. Representation of basal melting at the grounding line
670 in ice flow models. *Cryosphere* **12**, 3085–3096 (2018).
- 671 74. Reed, B., Green, J. A. M., Jenkins, A. & Gudmundsson, G. H. Model data for
672 ‘Recent irreversible retreat phase of Pine Island Glacier’. Zenodo
673 <https://doi.org/10.5281/zenodo.10043471> (2023).

674



..... Present day - - - - - No melt (500 yrs) ——— TC700 (100 yrs) ——— TC600 (50 yrs)

